J Appl Physiol 126: 1550–1562, 2019.
First published April 4, 2019; doi:10.1152/japplphysiol.00898.2018.

RESEARCH ARTICLE | *Translational Control of Muscle Mass*

Angiotensin II suppresses autophagy and disrupts ultrastructural morphology and function of mitochondria in mouse skeletal muscle

Kleiton Augusto Santos Silva,[1] Thaysa Ghiarone,[2] Kathy Schreiber,[3] DeAna Grant,[4] Tommi White,[4,5] Madlyn I. Frisard,[6] Sergiy Sukhanov,[1,8] Bysani Chandrasekar,[1,2,7,8] Patrice Delafontaine,[1,8] and Tadashi Yoshida[1,8]

[1]*Department of Medicine, University of Missouri School of Medicine, Columbia, Missouri;* [2]*Dalton Cardiovascular Research Center, University of Missouri, Columbia, Missouri;* [3]*Cell and Immunobiology Core, University of Missouri, Columbia, Missouri;* [4]*Electron Microcopy Core Facility, University of Missouri, Columbia, Missouri;* [5]*Department of Biochemistry, University of Missouri, Columbia, Missouri;* [6]*Department of Human Nutrition, Foods, and Exercise, Virginia Tech, Blacksburg, Virginia;* [7]*Research Service, Harry S. Truman Memorial Veterans' Hospital, Columbia, Missouri; and* [8]*Department of Medical Pharmacology and Physiology, University of Missouri School of Medicine, Columbia, Missouri*

Submitted 11 October 2018; accepted in final form 3 April 2019

Silva KA, Ghiarone T, Schreiber K, Grant D, White T, Frisard MI, Sukhanov S, Chandrasekar B, Delafontaine P, Yoshida T. Angiotensin II suppresses autophagy and disrupts ultrastructural morphology and function of mitochondria in mouse skeletal muscle. *J Appl Physiol* 126: 1550–1562, 2019. First published April 4, 2019; doi:10.1152/japplphysiol.00898.2018.—Angiotensin II (ANG II)-induced skeletal muscle wasting is characterized by activation of the ubiquitin-proteasome system. However, the potential involvement of proteolytic system macroautophagy/autophagy in this wasting process remains elusive. Autophagy is precisely regulated to maintain cell survival and homeostasis; thus its dysregulation (i.e., overactivation or persistent suppression) could lead to detrimental outcomes in skeletal muscle. Here we show that infusion of ANG II for 7 days in male FVB mice suppressed autophagy in skeletal muscle. ANG II blunted microtubule-associated protein 1 light chain 3B (LC3B)-I-to-LC3B-II conversion (an autophagosome marker), increased p62/SQSTM1 (an autophagy cargo receptor) protein expression, and decreased the number of autophagic vacuoles. ANG II inhibited UNC-51-like kinase 1 via inhibition of 5′-AMP-activated kinase and activation of mechanistic target of rapamycin complex 1, leading to reduced phosphorylation of beclin-1^{Ser14} and Autophagy-related protein 14^{Ser29}, suggesting that ANG II impairs autophagosome formation in skeletal muscle. In line with ANG II-mediated suppression of autophagy, ANG II promoted accumulation of abnormal/damaged mitochondria, characterized by swelling and disorganized cristae and matrix dissolution, with associated increase in PTEN-induced kinase 1 protein expression. ANG II also reduced mitochondrial respiration, indicative of mitochondrial dysfunction. Together, these results demonstrate that ANG II reduces autophagic activity and disrupts mitochondrial ultrastructure and function, likely contributing to skeletal muscle wasting. Therefore, strategies that activate autophagy in skeletal muscle have the potential to prevent or blunt ANG II-induced skeletal muscle wasting in chronic diseases.

NEW & NOTEWORTHY Our study identified a novel mechanism whereby angiotensin II (ANG II) impairs mitochondrial energy metabolism in skeletal muscle. ANG II suppressed autophagosome formation by inhibiting the UNC-51-like kinase 1(ULK1)-beclin-1 axis, resulting in accumulation of abnormal/damaged and dysfunctional mitochondria and reduced mitochondrial respiratory capacity. Therapeutic strategies that activate the ULK1-beclin-1 axis have the potential to delay or reverse skeletal muscle wasting in chronic diseases characterized by increased systemic ANG II levels.

autophagosome; beclin-1; LC3B; mitochondrial respiration; proteolysis

INTRODUCTION

Systemic levels of angiotensin II (ANG II) are elevated in chronic diseases such as heart failure, chronic kidney disease, and cancer (13, 45, 67). We and others have previously shown that ANG II contributes to skeletal muscle wasting (45, 53, 58, 67), suggesting that persistently elevated ANG II levels worsen the prognosis of these patients. In fact, ANG II has been recently implicated as a master upstream regulator of cachexia in cancer patients (45). Multiple studies have shown that ANG II induces skeletal muscle proteolysis via activation of the ubiquitin-proteasome system (UPS) (7, 15, 53, 65, 67). The UPS and the macroautophagy system (hereafter referred to as autophagy) are the two major intracellular protein degradation pathways (5, 36, 54, 64), but the potential involvement of autophagy in ANG II-mediated skeletal muscle wasting remains elusive.

In autophagy, a double-membrane autophagy-related organelle (autophagosome) is formed to engulf different intracellular components (i.e., nonselective autophagy) or a specific intracellular structure (i.e., selective autophagy), where upon fusion with lysosomes its contents undergo hydrolase-dependent degradation (5, 24, 38, 55). Autophagy has been shown to induce skeletal muscle proteolysis during prolonged starvation, denervation, and cancer by excessive capture and accelerated degradation of autolysosomal contents (41, 54). Therefore, we initially hypothesized that ANG II would promote autophagy-mediated skeletal muscle proteolysis. Instead, we found that ANG II impairs the autophagy-initiating signaling pathway in skeletal muscle, leading to decreased autophagosome formation. It is highly likely that the reduced skeletal muscle autophagic flux impairs clearance of unwanted/damaged organelles such as mitochondria. In fact, our data show that the

Address for reprint requests and other correspondence: T. Yoshida, Dept. of Medicine, Univ. of Missouri School of Medicine, One Hospital Dr., M742, Columbia, MO 65212 (e-mail: yoshidata@health.missouri.edu).

number of abnormal/damaged mitochondria was significantly increased in skeletal muscle after ANG II infusion. Importantly, mitochondrial aerobic respiration was severely impaired, likely causing decreased skeletal muscle energy production and wasting.

MATERIALS AND METHODS

Animals. All animal studies were reviewed approved by the Institutional Animal Care and Use Committee at the University of Missouri, Columbia and followed National Institutes of Health guidelines. Male FVB mice (10–12 wk old) purchased from The Jackson Laboratory (Bar Harbor, ME) were housed under standard laboratory conditions in which room temperature was 21–22°C and light and dark cycles were 12 h each. Animals were continuously infused with ANG II (Sigma-Aldrich, St. Louis, MO; no. A9525) dissolved in acidified saline (0.01 M acetic acid) at 1.0 $\mu g \cdot kg^{-1} \cdot min^{-1}$ via subcutaneously implanted osmotic minipumps (Durect, Cupertino, CA; Alzet no. 1007D) and euthanized at 12 h, 1 day, 4 days, or 7 days after ANG II infusion. Since ANG II markedly reduces food intake (7, 66), which may activate autophagy due to caloric restriction (10), we included a pair-fed (PF) group (saline infused and given the same amount of food as the ANG II group) as a control to exclude food intake-mediated effects on autophagy. All animals had free access to water, and all animals, except for the PF group, had free access to food throughout the study period. Body weight and food intake were measured daily. After a 3-day acclimatization period, systolic blood pressure (SBP) was measured from *day 2* to *day 6* of ANG II infusion by tail-cuff plethysmography (BP-2000 System, Visitech Systems, Apex, NC). For the autophagic flux evaluation at 1 day or 7 days of ANG II infusion, the PF and ANG II groups received colchicine (0.4 $mg \cdot kg^{-1} \cdot day^{-1}$ ip; Sigma-Aldrich, no. C9754). Mice were treated with colchicine for 2 days before euthanasia (29), whereas control groups received saline.

Antibodies and immunoblotting. Tibialis anterior (TA) muscles were removed, weighed, snap-frozen in liquid nitrogen, and stored at −80°C until being processed. After pulverization, the TA muscles (~20 mg) were homogenized in 10 volumes of ice-cold RIPA buffer [50 mM Tris·HCl (pH 7.5), 150 mM NaCl, 0.1% SDS, 0.5% Na-deoxycholate, 1% Triton] containing freshly reconstituted protease and phosphatase inhibitors (Halt Protease and Phosphatase Inhibitor Single-use Cocktail 100X; Thermo Fisher Scientific, Waltham, MA; no. 78442). Tissue homogenates were incubated on ice for 30 min (vortexed every 10 min) and then centrifuged (15,000 *g* for 15 min at 4°C). The supernatants were collected, and the protein concentration was determined with the BCA Protein Assay Kit (Thermo Fisher Scientific; no. 23227). Proteins were separated in SDS-PAGE gels and transferred overnight onto PVDF membranes (0.22 μm or 0.45 μm). The membranes were blocked for 1 h at room temperature (RT) in 5% BSA or nonfat dry milk in Tris-buffered saline (TBS) plus 0.05% Tween-20 (TBS-T). The membranes were then incubated overnight at 4°C with primary antibodies diluted in 5% BSA or nonfat dry milk in TBS-T. After washing with TBS-T (3 × 10 min), the membranes were incubated with respective secondary antibodies diluted in 5% nonfat dry milk for 1 h at RT. After washing, the membranes were covered with the ECL chemiluminescence reagent (Thermo Fisher Scientific; no. 32106) and scanned with the ChemiDoc XRS+ System (Bio-Rad, Hercules, CA). The following antibodies were used: microtubule-associated protein 1 light chain 3B (LC3B, 1:1,000; no. L7543) and Autophagy-related protein 14 (ATG14, 1:1,000; no. A6358) from Sigma-Aldrich; p62/SQSTM1 (Sequestosome 1, 1:1,000; no. MABC32) and peroxisome proliferator-activated receptor gamma coactivator-1α (PGC-1α, 1:2,000; no. ST1202) from MilliporeSigma (Burlington, MA); phosphatidylinositol 3-kinase p100 Vacuolar protein sorting 34 (Vps34, 1:1,000; no. sc-365404) and PTEN-Induced Kinase 1 (PINK1, 1:1,000; no. sc-33796) from Santa Cruz Biotechnology (Dallas, TX); Beclin-1 (1:1,000; no. ab207612), Lysosomal Associated Membrane Protein 1 (LAMP1, 1:1,000; no. ab24170), and Cytochrome-*c* oxidase, complex IV mitochondrial loading control (1:1,000; no. ab16056) from Abcam (Cambridge, UK); Fission 1 (Fis1, 1:1,000; no. 10956-1-AP) from Proteintech (Rosemont, IL); phospho-beclin-1^{Ser15} (Ser14 in mice, 1:500; no. 254515) from Abbiotec (San Diego, CA); and phospho-p70 $S6K^{T389}$ (1:1,000; no. 9234), p70 S6K (1:1, 000; no. 2708); phospho-$S6^{Ser240/244}$ (1:1,000; no. 5364), S6 (1:1,000; no. 2217), phospho-$ATG14^{Ser29}$ (1:1,000; no. 96752), 5′-AMP-activated kinase (AMPK, 1:1,000; no. 2532), phospho-$AMPK^{Thr172}$ (1:1,000; no. 2535), UNC-51-like kinase 1 (ULK1, 1:1,000; no. 8054), phospho-$ULK1^{Ser317}$ (1:1,000; no. 12755), p-$ULK1^{S555}$ (1:1,000; no. 5869), phospho-$ULK1^{Ser757}$ (1:1,000; no. 6888), Mitofusin-2 (1:1,000; no. 9482), Optic Atrophy 1 (OPA1, 1:1,000; no. 80471), Cytochrome *c* (1:1,000; no. 136F3), and α-Tubulin (1:1,000; no. 9099) from Cell Signaling Technology (Danvers, MA).

Quantitative RT-PCR. Total RNA from pulverized TA muscles was isolated as previously described (61, 65). Expression of Macrotubule-Associated Protein 1 Light Chain 3β (Map1lc3b; no. PPM27261A-200) and p62/Sqstm1 (no. PPM28731F-200) was analyzed by quantitative RT-PCR and normalized to the expression of the housekeeping gene Hprt1 (no. PPM03559F-200) (12, 22). The PCR primers were obtained from Qiagen (Germantown, MD).

Cathepsin B and L activity assays. Cathepsin B and L activity assays were performed as previously described with minor modifications (4). Briefly, gastrocnemius muscle pulverized under liquid nitrogen (~15 mg) was homogenized in lysis buffer [in mM: 50 Tris·HCl (pH 7.5), 150 NaCl, 1 EDTA, 5 $MgCl_2$, and 0.5 DTT]. Cathepsin B+L activity was measured by mixing 20 μg of protein with 50 μl of cathepsin B and L reaction buffer (in mM: 100 mM acetate (pH 5.5), 1 EDTA, and 2 DTT] and 1 mM cathepsin B and L substrate Z-Phe-Arg-AMC (MilliporeSigma; no. 03-32-1501). Fluorescence intensity (excitation 380 nm; emission 460 nm) was measured in a kinetics-based assay for 90 min at 37°C with a Cytation 5 Cell Imaging Multi-Mode Reader (Biotek, Winooski, VT). For cathepsin L activity measurement, the same set of samples was incubated for 15 min at RT with cathepsin B inhibitor (MilliporeSigma; no. 219385) before the addition of cathepsin B+L substrate. Cathepsin B activity was calculated by subtracting the cathepsin L activity from the cathepsin B+L activity.

Isolation of enriched mitochondrial fraction. Mitochondria were isolated as described previously (6, 21), with minor modifications. Briefly, freshly isolated TA muscles were rinsed in ice-cold PBS, minced, and incubated in isolation buffer for mitochondria 1 [IBm1; in mM: 67 sucrose, 50 Tris·HCl (pH 7.4), 50 KCl, and 10 EDTA, with 0.2% BSA] plus trypsin-EDTA (0.25%) for 30 min on ice. Then muscles were centrifuged at 200*g* for 3 min at 4°C. Muscles were manually homogenized in ice-cold IBm1 with a Kimble Kontes Dounce tissue grinder (30 strokes; Fisher Scientific, Hampton, NH; no. K885300) and centrifuged at 700*g* for 10 min at 4°C. The supernatants were collected and further centrifuged at 8,000*g* for 10 min at 4°C. The pellet was washed, suspended in IBm2 (in mM: 220 mannitol, 70 sucrose, 5 EGTA, and 10 Tris·HCl pH 7.4), and centrifuged at 8,000*g* for 10 min at 4°C. The final pellet (enriched mitochondrial fraction) was suspended in 100 μl of IBm2 and kept on ice until ready to use. Protein concentration was measured by the bicinchoninic method.

Mitochondria respiration assay (oxygen consumption rate). Mitochondrial oxygen consumption rate was assessed with XF^e96 Agilent Seahorse technology (Agilent, Santa Clara, CA). Enriched mitochondrial fractions were mixed in two different combinations of respiratory substrates and an inhibitor: pyruvate (10 mM) and malate (5 mM) for the complex I-mediated respiratory rates and succinate (10 mM) and rotenone (2 μM) for the complex II-mediated respiration rates. In the presence of the substrate-inhibitor combinations, mitochondria (2 μg and 1.5 μg for complex I and complex II assay, respectively) were seeded in the XF^e96 Agilent Seahorse culture plate and centrifuged at 2,000*g* for 20 min at 4°C. The culture plate was warmed at 37°C for

10 min and placed in the XF^{e}96 Agilent Seahorse machine. Oxygen consumption rate was measured by sequential injections of 5 mM ADP, 2 μM oligomycin, 4 μM carbonyl cyanide *p*-trifluoromethoxyphenylhydrazone (FCCP), and 4 μM antimycin A. The experiment was performed in three replicates per mouse for each respiratory substrate-inhibitor combination for the PF and ANG II groups after 7 days of infusion.

Skeletal muscle ultrastructural morphology. Ultrastructural morphology of extensor digitorum longus (EDL) muscle was analyzed by transmission electronic microscopy (TEM). After each experimental period, EDL muscle was harvested, weighed, and incubated in fixation solution (2% paraformaldehyde, 2% glutaraldehyde in 100 mM sodium cacodylate buffer pH 7.35) for 30 min (RT). After fixation, EDL muscle was rinsed with 100 mM sodium cacodylate buffer (pH 7.35) containing 130 mM sucrose. Secondary fixation was performed with 1% osmium tetroxide (Ted Pella, Redding, CA) in cacodylate buffer with a Pelco Biowave (Ted Pella) operated at 100 W for 1 min. After incubation at 4°C for 1 h, samples were rinsed with cacodylate buffer and further with distilled water. En bloc staining was performed with 1% aqueous uranyl acetate, incubated at 4°C overnight, and rinsed with distilled water. With the Pelco Biowave, a graded dehydration series (ethanol to acetone, 100 W for 40 s per exchange) was performed. Dehydrated tissues were then infiltrated with Epon resin (250 W for 3 min) and polymerized at 60°C overnight. Eighty-five-nanometer sections were cut with an ultramicrotome (Ultracut UCT; Leica Microsystems) and a diamond knife (Diatome, Hatfield, PA). Images were acquired with a JEOL JEM 1400 transmission electron microscope (JEOL, Peabody, MA) at 80 kV on a Gatan Ultrascan 1000 CCD (Gatan, Pleasanton, CA). Analysis of mitochondrial area and identification of abnormal mitochondria were performed by two investigators, one of whom was blinded to the identity of samples. Mitochondrial area was quantified with Olympus cellSens Dimension Desktop 1.13 (Olympus, Tokyo, Japan). Abnormal mitochondria were defined by *1*) total or partial disarrangements of the cristae, *2*) presence of matrix dissolution, and *3*) swollen shape, as characterized and described elsewhere (2, 14, 31). The term "autophagic vacuoles" was adopted to designate the morphological characteristics of autophagosomes and autolysosomes as described elsewhere (17). Autophagic vacuoles were identified and counted as previously reported (19, 63). Total autophagosome and autolysosome numbers were normalized per viewing field.

Statistical analysis. All data are presented as means ± SD, and a P value <0.05 is considered significant. Data were analyzed (GraphPad Prism, version 7) by Student's *t*-test (comparison between 2 experimental groups), one-way ANOVA followed by Tukey's multiple-comparison test (for comparison of 3 groups), and two-way ANOVA for nonrepeated measurements followed by Bonferroni's multiple-comparison test (for comparison of groups with 2 independent variables).

RESULTS

ANG II increases SBP and induces loss of skeletal muscle mass. Consistent with our previous studies (7, 59, 61, 66), ANG II infusion significantly increased SBP (Fig. 1*A*) and reduced food intake (Fig. 1*B*; ~52% reduction in ANG II compared with Sham at 7 days). A marked loss in total body weight was also observed upon ANG II infusion compared with Sham and PF groups (Sham 28.9 ± 2.5 g, PF 25.9 ± 1.3 g vs. ANG II 23.7 ± 2.8 g; $P < 0.05$, $n = 6$/group at 7 days). Notably, ANG II infusion resulted in a significant loss in skeletal muscle weight after 7 days in both gastrocnemius (Fig. 1*C*) and TA (Sham 48.5 ± 5.4 mg, PF 42.8 ± 2.1 mg vs. ANG II 38.2 ± 4.1 mg; $P < 0.05$, $n = 6$/group), whereas no such loss was observed after 12 h, 1 day, or 4 days of infusion (gastrocnemius in Fig. 1*D* and data not shown for TA; 12 h, $n = 5$; 1 day, $n = 6$; 4 days, $n = 6$; P = not significant, PF vs. ANG II).

ANG II impairs autophagic flux in skeletal muscle. Compared with the Sham group, the conversion from the diffused cytoplasmic form (LC3B-I) to the lipidated form (LC3B-II), hereafter referred as to LC3B conversion, was significantly increased (Fig. 2, *A* and *B*) and protein expression of p62 was decreased (Fig. 2, *A* and *C*) in the PF group, likely because of

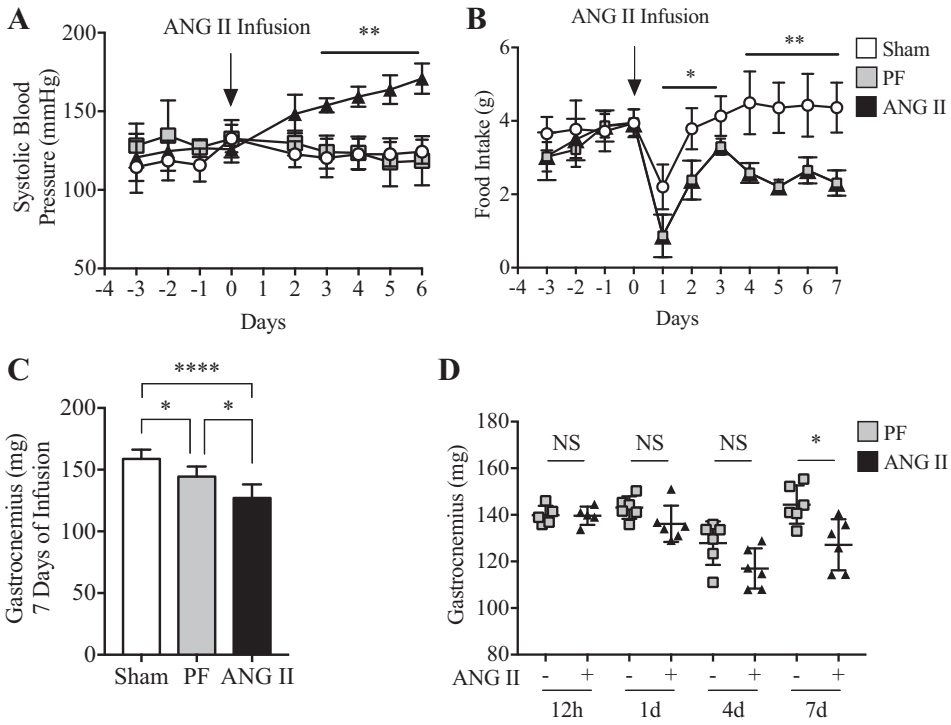

Fig. 1. ANG II infusion induces high blood pressure and the loss of skeletal muscle mass. *A*: ANG II (1.0 μg·kg^{-1}·min^{-1}) infusion increased systolic blood pressure. $n = 6$/group. **$P < 0.005$ for ANG II vs. Sham and pair fed (PF) groups from *day* 3 to *day 6*. *B*: ANG II decreased food intake throughout 7 days of experimental period. $n = 6$/group. *$P < 0.05$, **$P < 0.005$ from *day 1* to *day 7*; ~52% reduction at 7 days. *C*: gastrocnemius muscle mass at 7 days of ANG II infusion. $n = 6$/group. *$P < 0.05$ for Sham vs. PF and for PF vs. ANG II; ****$P < 0.0001$ for Sham vs. ANG II. *D*: gastrocnemius muscle mass measured in PF (−) and ANG II (+) groups at 12 h and 1, 4, and 7 days of infusion. $n = 5$/group and P = not significant (NS) for 12 h; $n = 6$/group and P = NS for 1 day; $n = 6$/group and P = NS for 4 days; $n = 6$/group and *$P < 0.05$ for 7 days]. Ten- to twelve-week old male FVB mice were used for all experiments. All data are means ± SD.

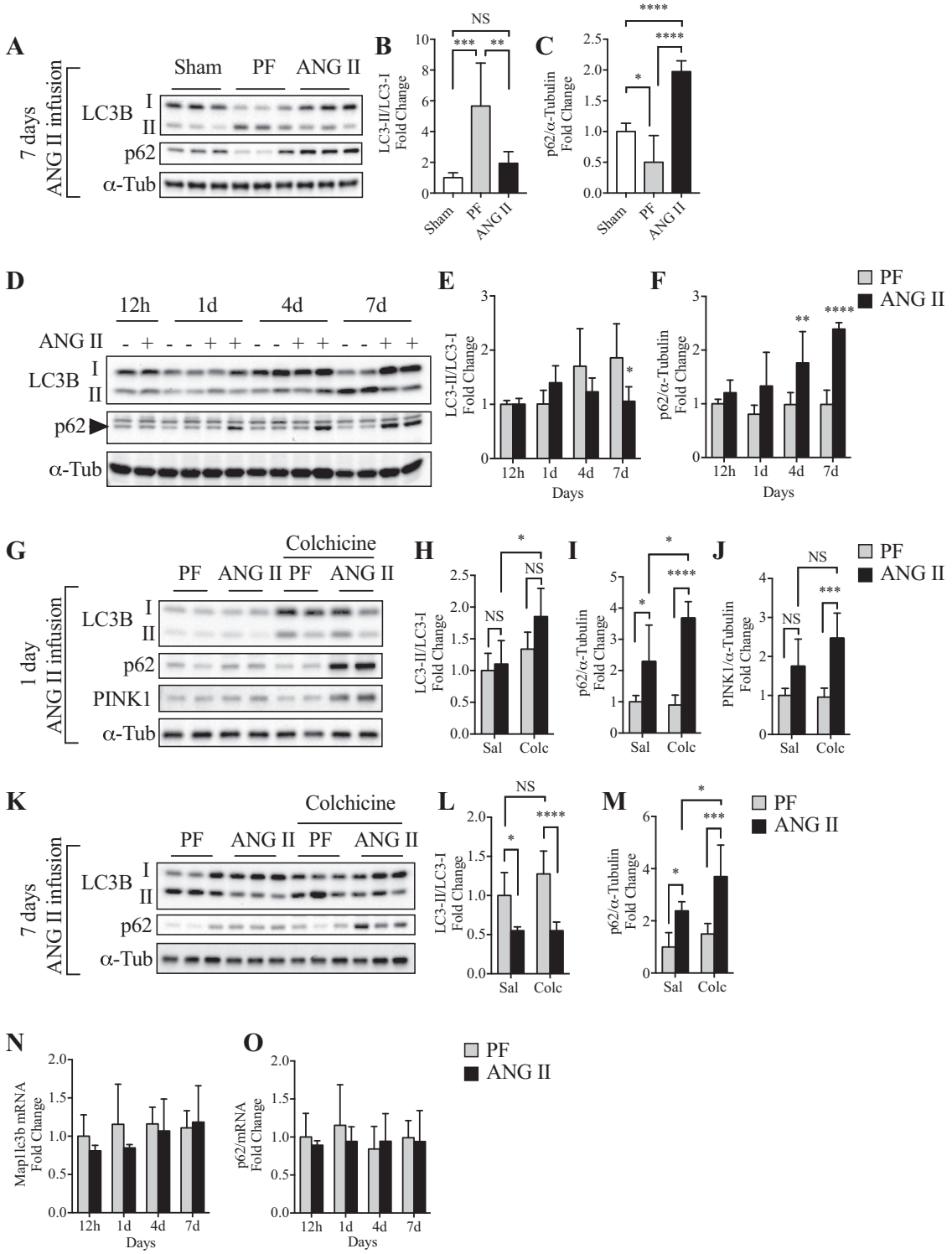

Fig. 2. ANG II infusion impairs autophagic flux in skeletal muscle. *A–C*: representative Western blots (*A*) and quantification of microtubule-associated protein 1 light chain 3B (LC3B)-I to LC3B-II conversion (*B*) and p62 expression (*C*) in Sham, pair-fed (PF), and ANG II groups after 7 days of infusion. LC3B-I to -II conversion was calculated as the ratio of lipidated form LC3B-II to cytosolic form LC3B-I. $n = 6$/group. α-Tub, α-tubulin. *D–F*: representative Western blots (*D*) and quantification of LC3B-I to LC3B-II conversion (*E*) and p62 expression (*F*) at 12 h and 1, 4, and 7 days of ANG II infusion. PF (−) and ANG II (+), $n = 3$/group for 12 h, 5/group for 1 day, 6/group for 4 and 7 days. *G–J*: representative Western blots (*G*) and quantification of LC3B-I to -II conversion (*H*), p62 expression (*I*), and PTEN-Induced Kinase 1 (PINK1) expression (*J*) after 1 day of ANG II infusion with (Colc) or without [saline (Sal)] colchicine treatment (0.4 $mg \cdot kg^{-1} \cdot day^{-1}$). $n = 6$/group. *K–M*: representative Western blots (*K*) and quantification of LC3B-I to LC3B-II conversion (*L*) and p62 expression (*M*) after 7 days of ANG II infusion with or without colchicine treatment. $n = 6$/group. *N* and *O*: quantitative RT-PCR of Macrotubule-Associated Protein 1 Light Chain 3β (Map1lc3b) (*N*) and p62/Sequestosome 1 (*O*) at 12 h and 1, 4, and 7 days of ANG II infusion. PF (−) and ANG II (+), $n = 3$/group for 12 h, 5/group for 1 day, 6/group for 4 and 7 days. α-Tub was used as loading control. Ten- to twelve-week-old male FVB mice were used for all experiments. All data are means ± SD. $^*P < 0.05$, $^{**}P < 0.005$, $^{***}P < 0.0005$, $^{****}P < 0.0001$. NS, nonsignificant.

caloric restriction-mediated autophagy activation. Furthermore, ANG II infusion inhibited LC3B conversion to levels similar to that seen in the Sham group (Fig. 2, *A* and *B*). However, a marked increase in p62 levels was observed after ANG II infusion compared with Sham and PF groups (Fig. 2, *A* and *C*). Detailed time course analysis revealed dynamic changes in LC3B conversion and p62 level (12 h to 7 days of infusion; Fig. 2, *D–F*). Although LC3B conversion was gradually increased in PF, ANG II blunted this increase. In contrast, p62 level remained constant in PF throughout the experimental period, whereas ANG II gradually increased p62 (Fig. 2, *D* and *F*). It has been reported that analysis of static levels of LC3B-II- to-LC3B-I ratio may be misleading because LC3B conversion and subsequent degradation are dynamically regulated (29). To further confirm the effect of ANG II on autophagic activity, animals were treated (for 2 days) with colchicine, an autophagic flux blocker (29, 37), after 1 day or 7 days of ANG II infusion. Although a trend in increase in LC3B conversion in the ANG II+colchicine group was observed compared with PF+colchicine at 1 day, it was not statistically significant (Fig. 2, *G* and *H*; $n = 6$/group, $P = 0.08$). ANG II increased p62 (Fig. 2, *G* and *I*) and PINK1 (Fig. 2, *G* and *J*) levels in the presence of colchicine. At a later stage of ANG II infusion (7 days), colchicine treatment further confirmed that ANG II blocked the autophagic flux, as evidenced by an inhibition in LC3B conversion (Fig. 2, *K* and *L*) and increased p62 accumulation (Fig. 2, *K* and *M*). Of note, LC3B and p62 mRNA levels were not altered by ANG II (Fig. 2, *N* and *O*), indicating that these changes in autophagy markers are regulated at the posttranscriptional level. To further demonstrate that ANG II impairs autophagy, we quantified the number of autophagic vacuoles (i.e., autophagosomes and autolysosomes) in EDL muscles by TEM. Since low numbers of autophagic vacuoles were observed by TEM (data not shown and Fig. 3*C*), the animals were treated with colchicine to block autophagic flux. Under this condition, ANG II-infused mice showed a significant reduction in the number of autophagic vacuoles compared with PF mice in both subsarcolemmal and intramyofibrillar areas (Fig. 3). These data are consistent with reduced LC3B conversion and increased p62 levels (Fig. 2) and together indicate that ANG II induces mitochondria depolarization as early as 24 h of infusion but fails to induce autophagosome formation.

Lysosome function is not altered in ANG II-infused mice. Having demonstrated that ANG II inhibits autophagosome formation (Figs. 2 and 3), we next determined whether ANG II regulates lysosomal content and/or function. LAMP1 and LAMP2 comprise ~50% of total lysosome proteins (18). The data show no significant difference in LAMP1 protein expression between ANG II and PF groups (Fig. 4, *A* and *B*),

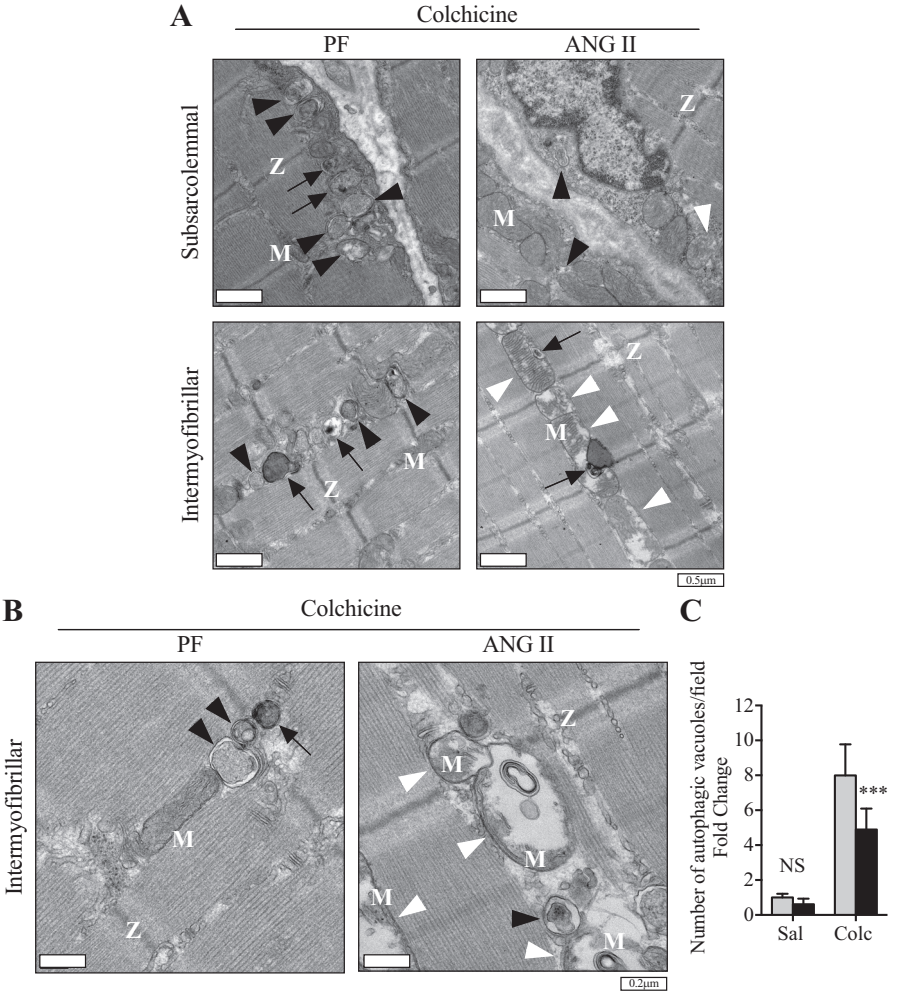

Fig. 3. ANG II reduces the number of autophagic vacuoles. *A*: representative transmission electronic micrographs from extensor digitorum longus (EDL) muscle of pair-fed (PF; *left*) and ANG II (*right*) groups of subsarcolemmal area (*top*) and intramyofibrillar area (*bottom*). *B*: representative transmission electronic micrographs from EDL muscle of PF and ANG II groups in the intramyofibrillar area at higher magnification. M, mitochondria; Z, Z lines (which delimit a sarcomere). White arrowheads indicate abnormal mitochondria, characterized by swollen shape, disorganized cristae, and matrix dissolution. Black arrowheads indicate autophagosomes, and black arrows indicate autolysosomes. *C*: quantification of autophagic vacuoles in PF and ANG II groups with (Colc) or without [saline (Sal)] colchicine (0.4 $mg \cdot kg^{-1} \cdot day^{-1}$). $n = 6$/group. Ten- to twelve-week-old male FVB mice were used for all experiments. All data are means ± SD. $***P < 0.0005$. NS, nonsignificant.

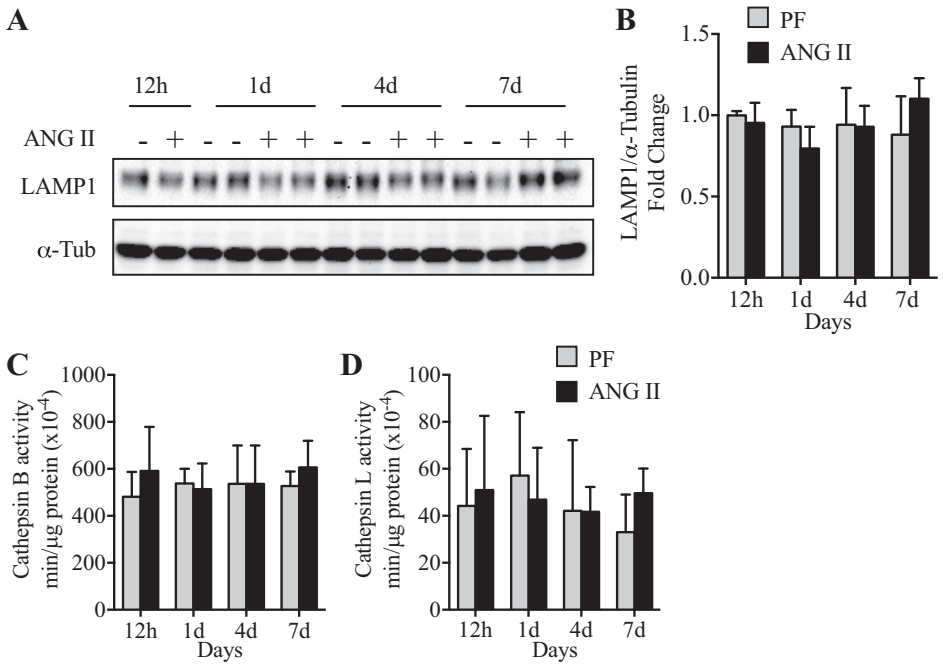

Fig. 4. ANG II did not alter lysosomal content or enzymatic activity. *A* and *B*: representative Western blot (*A*) and quantification (*B*) of Lysosomal-associated membrane protein 1 (LAMP1) in tibialis anterior (TA) muscle in pair-fed [PF (−)] and ANG II (+) mice at 12 h and 1, 4, and 7 days of ANG II infusion. α-Tubulin (α-Tub) was used as loading control. *C* and *D*: enzymatic activity of Cathepsin B (*C*) and L (*D*) in TA muscle of mice infused with ANG II for 12 h and 1, 4, and 7 days. Ten- to twelve-week-old male FVB mice were used for all experiments. All data are means ± SD. $n = 3$ for 12 h, 5 for 1 day, and 6 for 4 and 7 days.

suggesting that ANG II did not alter lysosomal content. Furthermore, no difference in lysosomal enzymatic activity (cathepsins B+L) was detected between ANG II and PF groups (Fig. 4, *C* and *D*). These data indicate that decreased autophagic flux after ANG II infusion is not associated with altered lysosomal content or activity.

Signaling pathways involved in autophagosome formation are disrupted in ANG II-infused mice. AMPK and mechanistic target of rapamycin complex 1 (mTORC1) regulate autophagy induction (30). Our data show that although ANG II reduced phosphorylation of AMPK (Thr172) compared with PF at 4 days (Fig. 5, *A* and *B*), it increased phosphorylation of mTORC1 downstream targets S6K1 (Thr389) at 4 and 7 days and S6 (Ser240/244) at 7 days (Fig. 5, *A*, *C*, and *D*). It has been previously reported that although AMPK induces ULK1 phosphorylation at Ser317 and Ser555, mTORC1 induces ULK1 phosphorylation at Ser757. Our data show that ANG II reduced p-ULK1 (Ser317) at 7 days (Fig. 5, *E* and *F*), while p-ULK1 (Ser555) was not altered (Fig. 5, *E* and *G*; at 4 days $P = 0.10$). In contrast, p-ULK1 (Ser757) was increased at 4 days (Fig. 5, *E* and *H*). After ULK1 activation, the VPS34 forms a complex (VPS34-VPS15-beclin-1-ATG14) to initiate autophagosome formation (i.e., the isolation membrane). Although VPS34 protein level was not altered by ANG II (Fig. 5, *I* and *L*), an increase in p-beclin-1 (Ser14) was detected in the PF group, likely because of reduced food intake and mTORC1 inhibition, and ANG II blunted this increase (Fig. 5, *I* and *J*). Furthermore, ANG II decreased p-ATG14 (Ser29) levels (Fig. 5, *I* and *K*).

ANG II causes accumulation of abnormal mitochondria in skeletal muscle. Defective autophagy can be detrimental to skeletal muscle and may lead to accumulation of intracellular waste of damaged and dysfunctional organelles such as mitochondria (i.e., reduced mitophagy) (23, 48). To determine whether ANG II-mediated impairment of autophagy induces morphological changes and/or dysfunction of mitochondria, we analyzed mitochondrial ultrastructure by TEM. We observed ~3% of abnormal mitochondria (swollen shape and having disorganized cristae and matrix dissolution) in the PF group throughout the experimental period (Fig. 6, *A* and *C*). ANG II did not alter the number of abnormal mitochondria at earlier time points of infusion (Fig. 6*A*; 12 h, 1 days, and 4 days), but it increased significantly after 7 days of infusion (~10%, Fig. 3, *A* and *B*, and Fig. 6, *A*–*C*). Furthermore, ANG II shifted the frequency distribution of mitochondrial size toward larger mitochondria (Fig. 6*D*) and increased average mitochondrial area (Fig. 6*E*). Importantly, mitochondria from the ANG II group had decreased number of cristae (Fig. 6*F*) and length of each crista (Fig. 6*G*).

Skeletal muscle from ANG II-infused mice display reduced aerobic respiratory capacity. To evaluate whether the increase in the number of abnormal mitochondria observed by TEM is associated with decreased function of this organelle, we analyzed mitochondrial respiration with the Seahorse XF^{e}96 analyzer. Although ANG II infusion did not affect basal respiratory rates (state II or pseudo-state IV), maximal ADP-stimulated respiration (state III_{ADP}) and FCCP-stimulated maximal respiration were decreased in the ANG II group in the complex I assay (Fig. 7*A*). With regard to complex II-mediated mitochondrial respiration, we found a significant decrease in basal respiratory rates (state II) and a low respiratory capacity in state III_{ADP} stimulation and in FCCP-stimulated maximal respiration in the ANG II group (Fig. 7*B*). Consistent with the lowered mitochondrial respiratory capacity, the mitochondrial cytochrome *c* level was reduced in the ANG II group (Fig. 7, *C* and *D*). One consequence of defects in the mitochondrial respiratory chain is the inability to maintain ionic gradients across the mitochondrial inner membrane, leading to membrane depolarization. PINK1 is selectively stabilized on depolarized mitochondria to activate Parkin, which promotes PINK1/Parkin-dependent mitophagy. Consistently, an increase in PINK1 expression was detected in whole tissue lysates as early as 1 day (detected in the presence of colchicine; Fig. 2, *G*

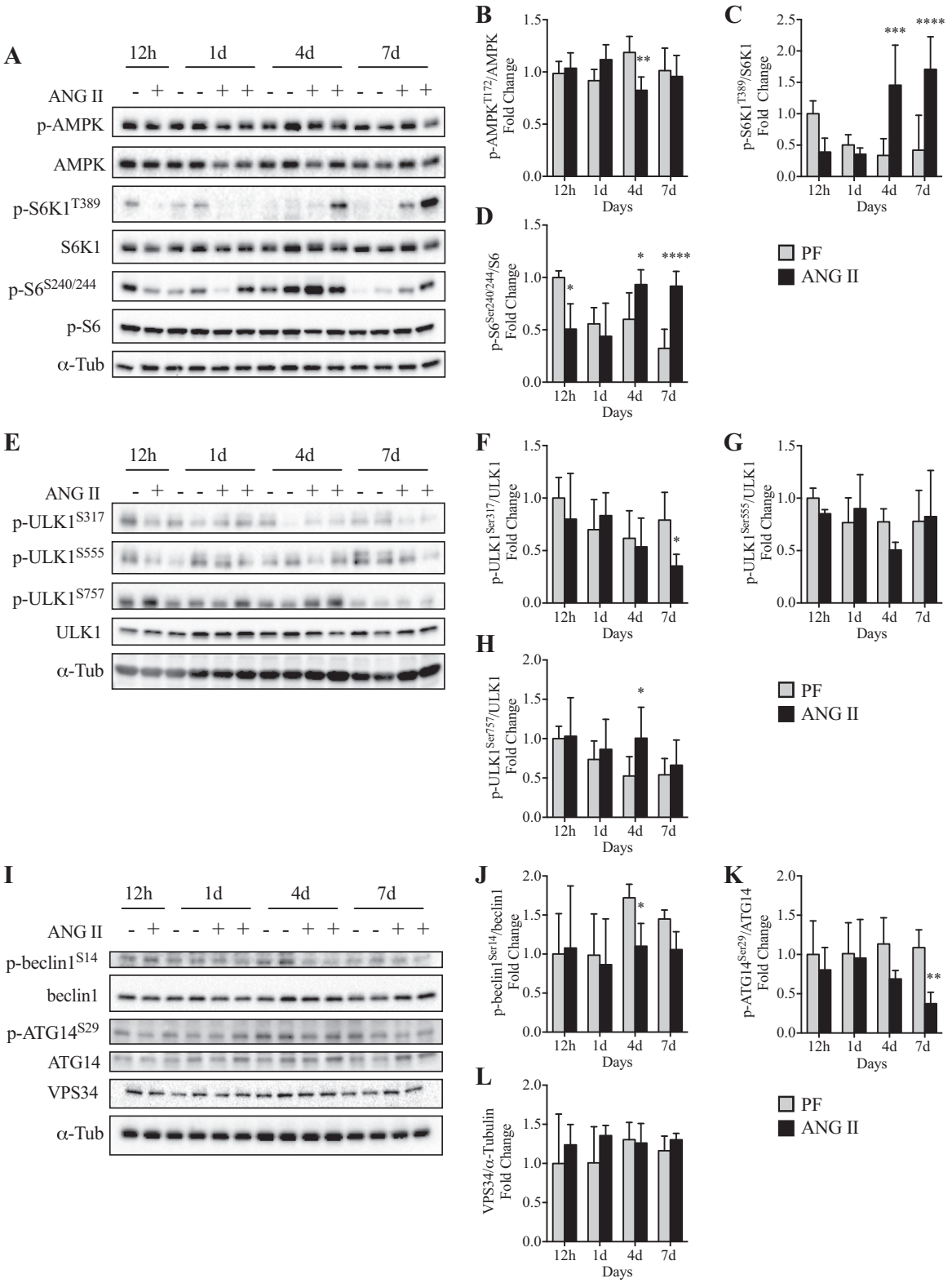

Fig. 5. ANG II infusion negatively regulates beclin-1-Vacuolar protein sorting 34 (VPS34)-Autophagy-related protein 14 (ATG14) complex via 5′-AMP-activated kinase (AMPK)-mechanistic target of rapamycin complex 1 (mTORC1) axis. *A–D*: representative Western blots (*A*) and quantification of phosphorylated (p)-AMPK/AMPK (*B*), p-S6K1/S6K1 (*C*), and p-S6/S6 (*D*) at 12 h and 1, 4, and 7 days in pair-fed [PF (−)] and ANG II-infused (+) mice. $n = 6$/group for 12 h and 1 d and 8/group for 4 and 7 days. *E–H*: representative Western blots (*E*) and quantification of p-UNC-51-like kinase 1 (ULK1)^{S317}/ULK1 (*F*), p-ULK1^{S757}/ULK1 (*G*), and p-ULK1^{S555}/ULK1 (*H*) in PF (−) and ANG II-infused (+) mice. $n = 3$/group for 12 h, 5/group for 1 day, 6/group for 4 and 7 days. *I–L*: representative Western blots (*I*) and quantification of p-Beclin-1^{S14}/beclin-1 (*J*), p-ATG14^{S29}/ATG14 (*K*), and VPS34/α-tubulin (*L*) at 12 h and 1, 4, and 7 days in PF (−) and ANG II-infused (+) mice. $n = 3$ for 12 h, 5 for 1 day, 6 for 4 and 7 days. α-Tubulin (α-Tub) was used as loading control. Ten- to twelve-week-old male FVB mice were used for all experiments. All data are means ± SD. $^*P < 0.05$, $^{**}P < 0.005$, $^{***}P < 0.0005$, $^{****}P < 0.0001$.

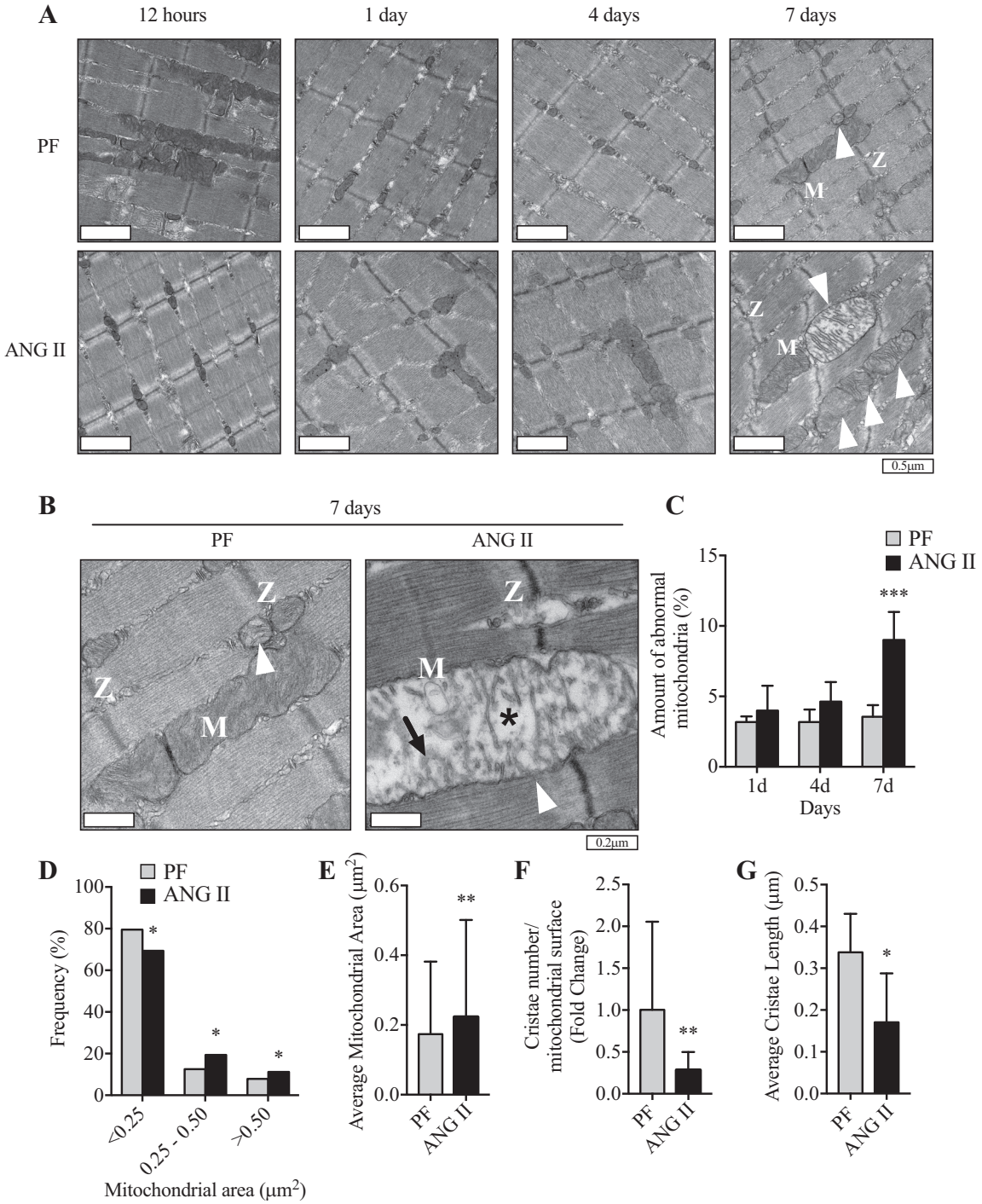

Fig. 6. ANG II infusion leads to accumulation of abnormal mitochondria. *A*: representative transmission electronic micrographs at lower magnification from extensor digitorum longus (EDL) muscle of pair-fed (PF; *top*) and ANG II-infused (*bottom*) mice at 12 h and 1, 4, and 7 days. *B*: higher-magnification images at 7 days of infusion. M, mitochondria; Z, Z lines (which delimit a sarcomere). White arrowheads indicate abnormal mitochondria, characterized by swollen shape, disorganized cristae (indicated by black arrow), and matrix dissolution (indicated by asterisk). *C*: ratio of abnormal mitochondria to total mitochondrial number in EDL muscle of PF and ANG II-infused mice at 1, 4, and 7 days. $n = 5$ or 6/group. *D*: frequency distribution of mitochondrial area in EDL muscle of PF and ANG II mice at 7 days of ANG II infusion. $n = 6$/group. *E*: average mitochondrial area from EDL muscle in PF and ANG II groups at 7 days of ANG II infusion. $n = 6$ mice/group. *F*: number of cristae normalized by average mitochondrial surface area in PF and ANG II groups after 7 days of infusion. $n = 6$/group. *G*: average of mitochondrial crista length in PF and ANG II groups after 7 days of infusion. $n = 6$/group. Ten- to twelve-week-old male FVB mice were used for all experiments. All data are means ± SD. $n = 3$ for 12 h, 5 for 1 day, 6 for 4 and 7 days. $^*P < 0.05$, $^{**}P < 0.005$, $^{***}P < 0.0005$. Student's *t*-test for *E*–*G*.

and *J*) and remained at these levels at 4 and 7 days after ANG II infusion (Fig. 7, *E* and *F*). Increased PINK1 accumulation was also observed in isolated mitochondria from the ANG II group (Fig. 7, *G* and *H*). In addition, ANG II reduced protein levels of PGC-1α (Fig. 7, *I* and *J*) and Mitofusin2 (Mfn2) at 4 and 7 days, OPA1 at 7 days, and Fis1 at 4 and 7 days (Fig. 7, *I* and *K–M*).

DISCUSSION

Our initial hypothesis that ANG II would increase autophagy in skeletal muscle was proven to be incorrect. We found that ANG II infusion blunted LC3B conversion, increased p62 and PINK1 protein expression (Figs. 2 and 7), decreased autophagic vacuole formation, and promoted accumulation of abnormal mitochondria in skeletal muscle (Figs. 3 and 6). Moreover, ANG II infusion diminished oxidative phosphorylation (OXPHOS) of mitochondria (Fig. 7). Together, these data strongly suggest that ANG II impairs autophagy (9, 37, 38) and skeletal muscle energy metabolism.

In our ANG II infusion model, dynamic changes in autophagy-regulating molecules were observed throughout the experimental period, which underscores the importance of time course analyses to assess changes in autophagy in vivo. Importantly, our data showed that PINK1 and p62 were increased in the ANG II+colchicine group after 1 day (Fig. 2, *G*, *I*, and *J*). Increased PINK1 indicates that ANG II-induced mitochondrial depolarization (39, 46, 60) occurs as early as 1 day and suggests that the slight (but not statistically significant) increase in LC3B conversion at this time may be due to a compensatory mechanism to degrade depolarized mitochondria via mitophagy. However, autophagy was not sufficiently activated, as indicated by reduced LC3B-I to -II conversion and by accumulation of p62 at later time points. TEM analyses revealed a reduction in the number of autophagic vacuoles in the ANG II group, further supporting the observation that ANG II suppresses autophagic activity and mitophagy, ultimately impairing skeletal muscle energy homeostasis. In fact, persistent reduction in autophagic activity compromising skeletal muscle has been reported in several genetic muscle disorders such as collagen VI muscular dystrophy, Pompe disease, and Danon disease (23, 34, 40, 47, 57). In these pathophysiological conditions, blunted autophagic flux suppresses degradation of unwanted intracellular contents, leading to myopathy. Similar to mitochondrial abnormalities reported in these conditions, the ANG II infusion model strongly suggests that a reduction in autophagic flux and cargo degradation may be the underlying cause of skeletal muscle wasting in this model.

The reduction in autophagosome formation in the ANG II group is most likely due to inhibition of AMPK and activation of mTORC1 signaling, resulting in inhibition of ULK1, a serine-threonine kinase involved in autophagy during stress (16, 30). It has been shown that AMPK and mTORC1 differentially regulate initial stages of the autophagosome formation: AMPK activation initiates autophagy, whereas activation of mTORC1 decreases autophagy (9, 16). AMPK and mTORC1 coordinately regulate ULK1 activity via different phosphorylation sites: AMPK may activate ULK1 by phosphorylating at serine residues 317, 555, 467, and 777, whereas mTORC1 may downregulate ULK1 via phosphorylation of Ser757 (9, 16). Here we report that ANG II increased Ser757 phosphorylation of ULK1 (mTORC1 site) but decreased Ser317 phosphorylation (AMPK site), both of which would result in reduced ULK1 activity. Interestingly, we did not observe changes in ULK1 phosphorylation at Ser555 (also an AMPK site). It has been shown that ULK1 site phosphorylation by AMPK depends on the primary stimuli: Ser317 and Ser777 phosphorylation of ULK1 is required for its activation and autophagy upon glucose withdrawal, whereas Ser555 phosphorylation is critical during amino acid starvation (30, 44, 49, 51), although the precise mechanism of these AMPK-mediated differential ULK1 phosphorylation sites is unclear and warrants further investigations to help us better understand the exact skeletal muscle metabolic changes caused by ANG II.

AMPK has been shown to negatively regulate mTORC1 activity by phosphorylation of Tuberous Sclerosis Complex Subunit 2 (TSC2) and Regulatory Associated Protein of MTOR Complex 1 (Raptor), and mTORC1-dependent ULK1 phosphorylation at Ser757 is shown to disrupt ULK1-AMPK interaction, thus forming a negative feedback loop (30, 52). Once the cellular energy is depleted, AMPK is activated and inhibits mTORC1 activity and ULK1 phosphorylation at Ser757. It is interesting that Ser757 phosphorylation of ULK1 preceded that of Ser317, which may indicate that ANG II-mediated alteration of the AMPK-mTORC1 axis is initiated by activation of the mTORC1 pathway. The changes in the AMPK-mTORC1 axis will likely lead to reduced ULK1 activity and VPS34 complex formation, critical steps involved in initiating the autophagosome formation (3, 51). Among the several VPS34 complexes, the proautophagic complex that regulates autophagosome formation comprises VPS15, beclin-1, and ATG14 (3). Upon ULK1 activation, beclin-1 is phosphorylated at Ser14, leading to activation of the proautophagic beclin-1-VPS34-ATG14 complex (51). ATG14 determines the role of VPS34 complex in the assembly of the autophagosome, and ULK1 activates ATG14 via Ser29 phosphorylation (42). Consistent with the reduced ULK1 activity, we found that ANG II reduced phosphorylation of beclin-1 at Ser14 and ATG14 at Ser29 (Fig. 5). Together, these data indicate that ANG II impairs the initial signaling involved in autophagy activation. Moreover, they suggest that reduced activity of the beclin-1-VPS34-ATG14 complex may be the critical underlying mechanism of ANG II-mediated suppression of autophagosome formation and autophagic activity.

Upon mitochondrial damage (e.g., mitochondrial depolarization), PINK1 is selectively accumulated/stabilized on the outer mitochondrial membrane and recruits Parkin, which induces ubiquitination of mitochondrial proteins (33, 39). Tagged depolarized mitochondria can then be recognized by autophagosome receptors such as p62 for later degradation by the autolysosome (62). Our data show that ANG II caused a sustained increase in mitochondrial PINK1 expression (Fig. 2, *G* and *J*, and Fig. 7, *E–H*), which strongly suggests that the proper clearance of unwanted mitochondria is reduced within 24 h of ANG II infusion and, importantly, persists throughout the experimental period. This is likely the cause for the accumulation of abnormal mitochondria (swollen shape with reduced number and shorter length of cristae as well as the presence of matrix dissolution) seen in TEM micrographs (Figs. 3 and 6). It is of note that whereas a larger size could indicate healthier mitochondria, this is not likely the case in the ANG II infusion model because we found reduced expression of mitochondrial dynamics markers (Mfn2, OPA1, and Fis1),

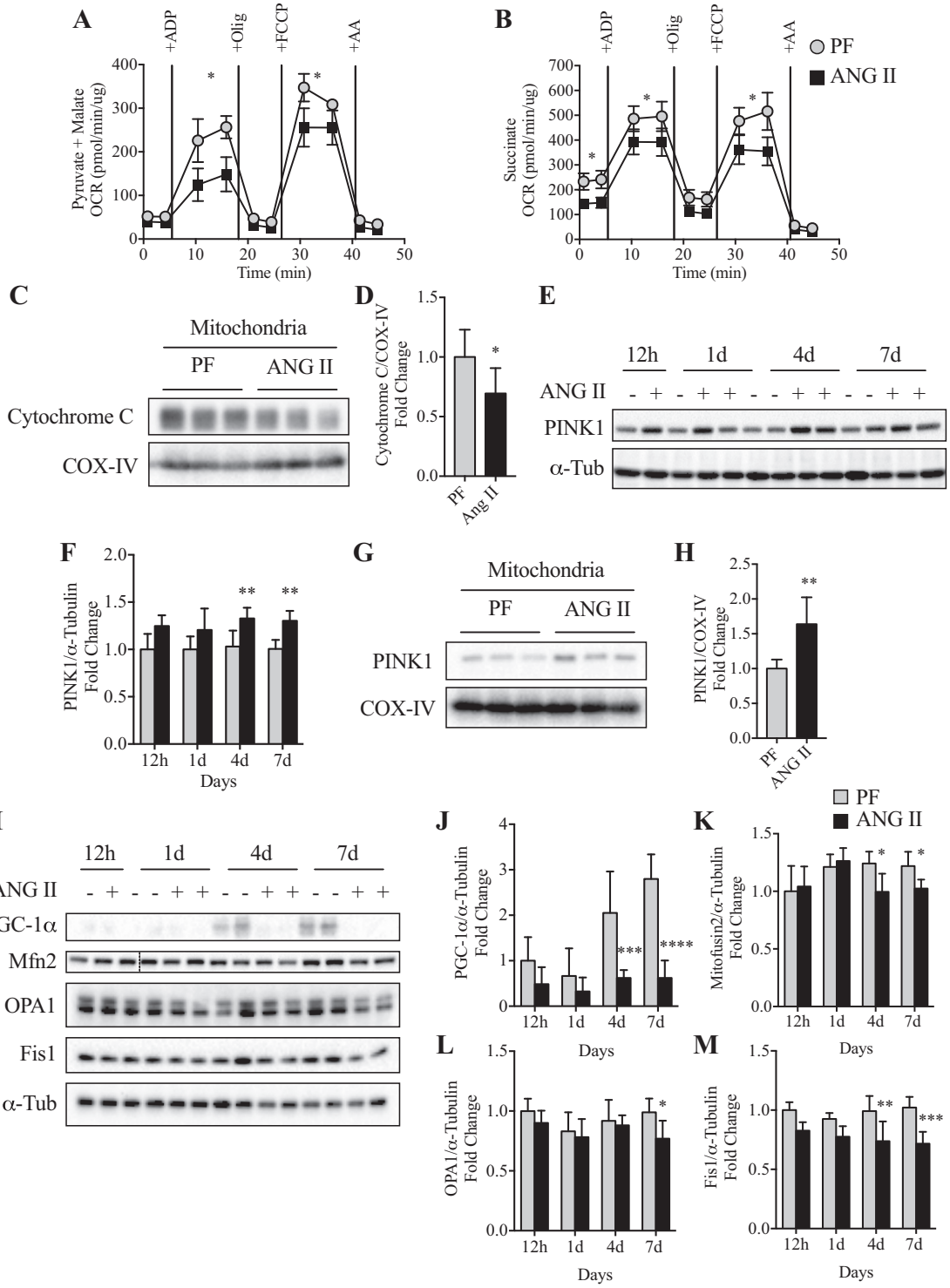

Fig. 7. ANG II infusion impairs mitochondrial bioenergetics in skeletal muscle. *A* and *B*: oxygen consumption rate (OCR) of complex I (*A*; in presence of 10 mM pyruvate + 5 mM malate)- and complex II (*B*; in presence of 10 mM succinate + 2 μM rotenone)-mediated respiration was measured in isolated skeletal muscle mitochondria at 7 days of ANG II infusion. $n = 6$/group. Olig, oligomycin; FCCP, carbonyl cyanide *p*-trifluoromethoxyphenylhydrazone; AA, antimycin A. *C* and *D*: representative Western blot (*C*) and quantification (*D*) of cytochrome *c* and cytochrome-*c* oxidase, complex IV (COX-IV) protein expression in enriched mitochondrial fraction from tibialis anterior (TA) muscle at 7 days of infusion. $n = 6$/group. *E* and *F*: representative Western blot (*E*) and quantification (*F*) of PTEN-Induced Kinase 1 (PINK1) protein expression at 12 h and 1, 4, and 7 days in PF (−) and ANG II (+) mice. $n = 3$/group for 12 h, 5/group for 1 day, 6/group for 4 and 7 days. *G* and *H*: representative Western blot (*G*) and quantification (*H*) of PINK1 protein expression in enriched isolated mitochondria fraction at 7 days of ANG II infusion. $n = 6$/group. *I*: representative Western blot images of peroxisome proliferator-activated receptor gamma coactivator-1α (PGC-1α), mitofusin2 (Mfn2), Optic Atrophy 1 (OPA1), and Fission 1 (Fis1) in TA muscle of PF (−) and ANG II (+) groups at 12 h and 1, 4, and 7 days. *J*–*M*: quantification of PGC-1α (*J*), Mfn2 (*K*), OPA1 (*L*), and FIS1 (*M*) protein expression in TA muscle of PF and ANG II mice. $n = 3$ for 12 h, 5 for 1 day, 6 for 4 and 7 days. α-Tubulin (α-Tub) or COX-IV was used as loading control. Ten- to twelve week-old male FVB mice were used for all experiments. All data are means ± SD. $^*P < 0.05$, $^{**}P < 0.005$, $^{***}P < 0.0005$. Student's *t*-test for *D* and *H*.

which suggests impaired mitochondrial quality control (50). These mitochondrial morphological abnormalities in the ANG II group are similar to those reported in skeletal muscles with myopathy such as in Ullrich congenital muscular dystrophy and extraocular muscle under chronic progressive external ophthalmoplegia (1, 8) as well as in conditions of high-fat diet (32).

We also observed an association between abnormal mitochondria and reduced function, as ANG II significantly reduced the mitochondrial aerobic respiratory capacity (Fig. 7). It is interesting to note that we observed lowered basal mitochondrial respiration only in complex II (succinate dehydrogenase). It has been reported that a mutation in the *Sdha* gene, which is a subunit of complex II, may lead to development of skeletal muscle weakness and myopathy in patients (25, 27), which are features of reduced autophagic activity (55). The lowered mitochondrial respiration was also associated with reduced expression of cytochrome *c*, which participates in OXPHOS by accepting and transferring electrons from complex III to complex IV (43), along with reduced AMPK activity and PGC-1α expression (Figs. 5 and 7). AMPK/PGC-1α signaling is critical in sensing the energy status and links it to induction of transcriptional programs that control energy expenditure. AMPK/PGC-1α has also been shown to generate new mitochondria and improve muscle oxidative metabolism in healthy skeletal muscles (20, 26, 28, 35, 56). Furthermore, PGC-1α reduces oxidative stress by promoting the expression of antioxidant enzymes. Therefore, a reduced AMPK-PGC-1α axis might be the underlying cause of ANG II-mediated mitochondrial dysfunction. Importantly, we have previously shown that ANG II infusion reduces skeletal muscle ATP content, which likely contributes to skeletal muscle wasting (61).The present study strongly suggests that ATP depletion is due to decreased mitochondrial OXPHOS caused by increased mitochondrial damage and reduced clearance of damaged/dysfunctional mitochondria.

In summary, our data provide novel insights into the mechanism of ANG II-mediated skeletal muscle autophagy and energy metabolism. Taken together with our previous studies, ANG II activates UPS (7, 64) and decreases autophagy in skeletal muscle. It is interesting to note that increased UPS and reduced autophagy are associated with sarcopenia in aging, in which the renin-angiotensin system is known to be activated (11). These observations suggest that increased ANG II is the underlying cause not only of cachexia (45) but also of aging-associated sarcopenia. Importantly, our data indicate that the ULK1-beclin-1-VPS34 axis plays a central role in ANG II-mediated suppression of skeletal muscle autophagy and defect in mitochondrial metabolism (Fig. 8). Further studies are war-

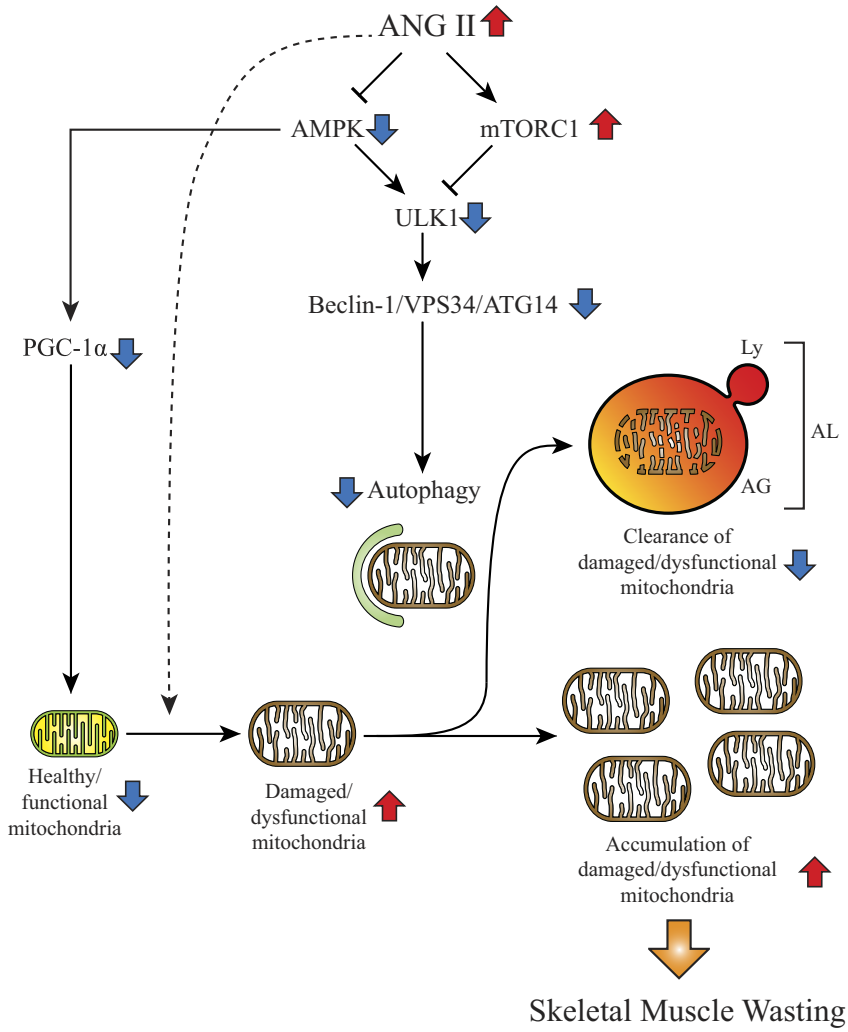

Fig. 8. Proposed mechanism of ANG II-mediated suppression of autophagy. Schematic illustration of how ANG II regulates autophagy by altering 5′-AMP-activated kinase (AMPK)-mechanistic target of rapamycin complex 1 (mTORC1) axis leading to reduction of autophagosome formation and induction of skeletal muscle wasting. Increased systemic levels of ANG II reduce AMPK-peroxisome proliferator-activated receptor γcoactivator-1α (PGC-1α) axis, which may reduce healthy mitochondria by inhibiting mitochondrial biogenesis and respiratory capacity. ANG II may also increase damaged/dysfunctional mitochondria via other mechanisms (e.g., oxidative stress, shown by dashed arrow). Under physiological conditions, damaged mitochondria are degraded by autophagy or mitophagy. However, elevated ANG II inhibits AMPK and stimulates mTORC1, which synergically inhibit UNC-51-like kinase 1 (ULK1) activity. Consequently, lowered ULK1 activity decreases phosphorylation of critical Vacuolar protein sorting 34 (VPS34) complex components [i.e., decreased phosphorylation of Ser14 residue of beclin-1 and Ser29 of Autophagy-related protein 14 (ATG14)]. Reduction of beclin-1-VPS34-ATG14 complex activity results in suppression of autophagosome formation, consequently decreasing autophagic flux. Therefore, damaged/dysfunctional mitochondria are not properly eliminated, and the accumulation of damaged/dysfunctional mitochondria consequently would lead to skeletal muscle wasting. The change of each component in the high-ANG II condition is shown by red (increase) and blue (decrease) arrows. AG, autophagosome; AL, autolysosome; Ly, lysosome.

ranted to target the ULK1-beclin-1 axis to develop a therapeutic approach to reverse skeletal muscle wasting in chronic diseases and aging that is associated with high levels of ANG II.

GRANTS

This study was supported by National Heart, Lung, and Blood Institute Grants R01 HL-080682 and R01 HL-070241 and National Institute of General Medical Sciences (NIGMS) Grants P30 GM-103337 and U54 GM-104940 to P. Delafontaine; American Heart Association (AHA) 15SDG25240022, NIGMS Grant P20 GM-103629, University of Missouri Research Council URC-18-012, a University of Missouri Department of Medicine Research Council grant, and a Kansas City Consortium of Musculoskeletal Diseases grant to T. Yoshida; AHA 18POST33960472 to K. A. S. Silva; and Department of Veterans Affairs Merit Award I01-BX004220 and Research Career Scientist Award IK6BX004016 to B. Chandrasekar.

DISCLOSURES

No conflicts of interest, financial or otherwise, are declared by the authors.

AUTHOR CONTRIBUTIONS

K.A.S.S. and T.Y. conceived and designed research; K.A.S.S. and D.G. performed experiments; K.A.S.S., T.G., K.S., D.G., T.W., M.I.F., and S.S. analyzed data; K.A.S.S. and T.Y. interpreted results of experiments; K.A.S.S. prepared figures; K.A.S.S. drafted manuscript; K.A.S.S., T.G., S.S., B.C., P.D., and T.Y. edited and revised manuscript; K.A.S.S., T.G., K.S., D.G., T.W., M.I.F., S.S., B.C., P.D., and T.Y. approved final version of manuscript.

REFERENCES

1. **Angelin A, Tiepolo T, Sabatelli P, Grumati P, Bergamin N, Golfieri C, Mattioli E, Gualandi F, Ferlini A, Merlini L, Maraldi NM, Bonaldo P, Bernardi P.** Mitochondrial dysfunction in the pathogenesis of Ullrich congenital muscular dystrophy and prospective therapy with cyclosporins. *Proc Natl Acad Sci USA* 104: 991–996, 2007. doi:10.1073/pnas.0610270104.
2. **Arismendi-Morillo G.** Electron microscopy morphology of the mitochondrial network in human cancer. *Int J Biochem Cell Biol* 41: 2062–2068, 2009. doi:10.1016/j.biocel.2009.02.002.
3. **Backer JM.** The intricate regulation and complex functions of the Class III phosphoinositide 3-kinase Vps34. *Biochem J* 473: 2251–2271, 2016. doi:10.1042/BCJ20160170.
4. **Baehr LM, West DW, Marshall AG, Marcotte GR, Baar K, Bodine SC.** Muscle-specific and age-related changes in protein synthesis and protein degradation in response to hindlimb unloading in rats. *J Appl Physiol (1985)* 122: 1336–1350, 2017. doi:10.1152/japplphysiol.00703.2016.
5. **Bonaldo P, Sandri M.** Cellular and molecular mechanisms of muscle atrophy. *Dis Model Mech* 6: 25–39, 2013. doi:10.1242/dmm.010389.
6. **Boutagy NE, Pyne E, Rogers GW, Ali M, Hulver MW, Frisard MI.** Isolation of mitochondria from minimal quantities of mouse skeletal muscle for high throughput microplate respiratory measurements. *J Vis Exp* 105: e53217, 2015. doi:10.3791/53217.
7. **Brink M, Wellen J, Delafontaine P.** Angiotensin II causes weight loss and decreases circulating insulin-like growth factor I in rats through a pressor-independent mechanism. *J Clin Invest* 97: 2509–2516, 1996. doi:10.1172/JCI118698.
8. **Carta A, D'Adda T, Carrara F, Zeviani M.** Ultrastructural analysis of extraocular muscle in chronic progressive external ophthalmoplegia. *Arch Ophthalmol* 118: 1441–1445, 2000. doi:10.1001/archopht.118.10.1441.
9. **Castets P, Frank S, Sinnreich M, Rüegg MA.** "Get the balance right": pathological significance of autophagy perturbation in neuromuscular disorders. *J Neuromuscul Dis* 3: 127–155, 2016. doi:10.3233/JND-160153.
10. **Choi AM, Ryter SW, Levine B.** Autophagy in human health and disease. *N Engl J Med* 368: 651–662, 2013. doi:10.1056/NEJMra1205406.
11. **Conti S, Cassis P, Benigni A.** Aging and the renin-angiotensin system. *Hypertension* 60: 878–883, 2012. doi:10.1161/HYPERTENSIONAHA.110.155895.
12. **de Kok JB, Roelofs RW, Giesendorf BA, Pennings JL, Waas ET, Feuth T, Swinkels DW, Span PN.** Normalization of gene expression measurements in tumor tissues: comparison of 13 endogenous control genes. *Lab Invest* 85: 154–159, 2005. doi:10.1038/labinvest.3700208.
13. **De Mello WC, Danser AH.** Angiotensin II and the heart: on the intracrine renin-angiotensin system. *Hypertension* 35: 1183–1188, 2000. doi:10.1161/01.HYP.35.6.1183.
14. **Divi RL, Haverkos KJ, Humsi JA, Shockley ME, Thamire C, Nagashima K, Olivero OA, Poirier MC.** Morphological and molecular course of mitochondrial pathology in cultured human cells exposed long-term to Zidovudine. *Environ Mol Mutagen* 48: 179–189, 2007. doi:10.1002/em.20245.
15. **Du Bois P, Pablo Tortola C, Lodka D, Kny M, Schmidt F, Song K, Schmidt S, Bassel-Duby R, Olson EN, Fielitz J.** Angiotensin II induces skeletal muscle atrophy by activating TFEB-mediated MuRF1 expression. *Circ Res* 117: 424–436, 2015. doi:10.1161/CIRCRESAHA.114.305393.
16. **Egan D, Kim J, Shaw RJ, Guan KL.** The autophagy initiating kinase ULK1 is regulated via opposing phosphorylation by AMPK and mTOR. *Autophagy* 7: 643–644, 2011. doi:10.4161/auto.7.6.15123.
17. **Eskelinen EL.** Maturation of autophagic vacuoles in mammalian cells. *Autophagy* 1: 1–10, 2005. doi:10.4161/auto.1.1.1270.
18. **Eskelinen EL.** Roles of LAMP-1 and LAMP-2 in lysosome biogenesis and autophagy. *Mol Aspects Med* 27: 495–502, 2006. doi:10.1016/j.mam.2006.08.005.
19. **Eskelinen EL.** To be or not to be? Examples of incorrect identification of autophagic compartments in conventional transmission electron microscopy of mammalian cells. *Autophagy* 4: 257–260, 2008. doi:10.4161/auto.5179.
20. **Finck BN, Kelly DP.** PGC-1 coactivators: inducible regulators of energy metabolism in health and disease. *J Clin Invest* 116: 615–622, 2006. doi:10.1172/JCI27794.
21. **Frisard MI, Wu Y, McMillan RP, Voelker KA, Wahlberg KA, Anderson AS, Boutagy N, Resendes K, Ravussin E, Hulver MW.** Low levels of lipopolysaccharide modulate mitochondrial oxygen consumption in skeletal muscle. *Metabolism* 64: 416–427, 2015. doi:10.1016/j.metabol.2014.11.007.
22. **Gong H, Sun L, Chen B, Han Y, Pang J, Wu W, Qi R, Zhang TM.** Evaluation of candidate reference genes for RT-qPCR studies in three metabolism related tissues of mice after caloric restriction. *Sci Rep* 6: 38513, 2016. doi:10.1038/srep38513.
23. **Grumati P, Coletto L, Sabatelli P, Cescon M, Angelin A, Bertaggia E, Blaauw B, Urciuolo A, Tiepolo T, Merlini L, Maraldi NM, Bernardi P, Sandri M, Bonaldo P.** Autophagy is defective in collagen VI muscular dystrophies, and its reactivation rescues myofiber degeneration. *Nat Med* 16: 1313–1320, 2010. doi:10.1038/nm.2247.
24. **He C, Klionsky DJ.** Regulation mechanisms and signaling pathways of autophagy. *Annu Rev Genet* 43: 67–93, 2009. doi:10.1146/annurev-genet-102808-114910.
25. **Hoekstra AS, Bayley JP.** The role of complex II in disease. *Biochim Biophys Acta* 1827: 543–551, 2013. doi:10.1016/j.bbabio.2012.11.005.
26. **Hoppeler H.** Molecular networks in skeletal muscle plasticity. *J Exp Biol* 219: 205–213, 2016. doi:10.1242/jeb.128207.
27. **Horváth R, Abicht A, Holinski-Feder E, Laner A, Gempel K, Prokisch H, Lochmüller H, Klopstock T, Jaksch M.** Leigh syndrome caused by mutations in the flavoprotein (Fp) subunit of succinate dehydrogenase (SDHA). *J Neurol Neurosurg Psychiatry* 77: 74–76, 2006. doi:10.1136/jnnp.2005.067041.
28. **Jäger S, Handschin C, St-Pierre J, Spiegelman BM.** AMP-activated protein kinase (AMPK) action in skeletal muscle via direct phosphorylation of PGC-1alpha. *Proc Natl Acad Sci USA* 104: 12017–12022, 2007. doi:10.1073/pnas.0705070104.
29. **Ju JS, Varadhachary AS, Miller SE, Weihl CC.** Quantitation of "autophagic flux" in mature skeletal muscle. *Autophagy* 6: 929–935, 2010. doi:10.4161/auto.6.7.12785.
30. **Kim J, Kundu M, Viollet B, Guan KL.** AMPK and mTOR regulate autophagy through direct phosphorylation of Ulk1. *Nat Cell Biol* 13: 132–141, 2011. doi:10.1038/ncb2152.
31. **Ko F, Abadir P, Marx R, Westbrook R, Cooke C, Yang H, Walston J.** Impaired mitochondrial degradation by autophagy in the skeletal muscle of the aged female interleukin 10 null mouse. *Exp Gerontol* 73: 23–27, 2016. doi:10.1016/j.exger.2015.11.010.
32. **Laker RC, Xu P, Ryall KA, Sujkowski A, Kenwood BM, Chain KH, Zhang M, Royal MA, Hoehn KL, Driscoll M, Adler PN, Wessells RJ, Saucerman JJ, Yan Z.** A novel MitoTimer reporter gene for mitochondrial content, structure, stress, and damage in vivo. *J Biol Chem* 289: 12005–12015, 2014. doi:10.1074/jbc.M113.530527.
33. **Lazarou M, Sliter DA, Kane LA, Sarraf SA, Wang C, Burman JL, Sideris DP, Fogel AI, Youle RJ.** The ubiquitin kinase PINK1 recruits

autophagy receptors to induce mitophagy. *Nature* 524: 309–314, 2015. doi:10.1038/nature14893.
34. **Masiero E, Agatea L, Mammucari C, Blaauw B, Loro E, Komatsu M, Metzger D, Reggiani C, Schiaffino S, Sandri M.** Autophagy is required to maintain muscle mass. *Cell Metab* 10: 507–515, 2009. doi:10.1016/j.cmet.2009.10.008.
35. **Mihaylova MM, Shaw RJ.** The AMPK signalling pathway coordinates cell growth, autophagy and metabolism. *Nat Cell Biol* 13: 1016–1023, 2011. doi:10.1038/ncb2329.
36. **Milan G, Romanello V, Pescatore F, Armani A, Paik JH, Frasson L, Seydel A, Zhao J, Abraham R, Goldberg AL, Blaauw B, DePinho RA, Sandri M.** Regulation of autophagy and the ubiquitin-proteasome system by the FoxO transcriptional network during muscle atrophy. *Nat Commun* 6: 6670, 2015. doi:10.1038/ncomms7670.
37. **Mizushima N, Yoshimori T.** How to interpret LC3 immunoblotting. *Autophagy* 3: 542–545, 2007. doi:10.4161/auto.4600.
38. **Mizushima N, Yoshimori T, Levine B.** Methods in mammalian autophagy research. *Cell* 140: 313–326, 2010. doi:10.1016/j.cell.2010.01.028.
39. **Narendra DP, Jin SM, Tanaka A, Suen DF, Gautier CA, Shen J, Cookson MR, Youle RJ.** PINK1 is selectively stabilized on impaired mitochondria to activate Parkin. *PLoS Biol* 8: e1000298, 2010. doi:10.1371/journal.pbio.1000298.
40. **Nascimbeni AC, Fanin M, Masiero E, Angelini C, Sandri M.** Impaired autophagy contributes to muscle atrophy in glycogen storage disease type II patients. *Autophagy* 8: 1697–1700, 2012. doi:10.4161/auto.21691.
41. **O'Leary MF, Hood DA.** Denervation-induced oxidative stress and autophagy signaling in muscle. *Autophagy* 5: 230–231, 2009. doi:10.4161/auto.5.2.7391.
42. **Obara K, Ohsumi Y.** Atg14: a key player in orchestrating autophagy. *Int J Cell Biol* 2011: 713435, 2011. doi:10.1155/2011/713435.
43. **Ow YP, Green DR, Hao Z, Mak TW.** Cytochrome *c*: functions beyond respiration. *Nat Rev Mol Cell Biol* 9: 532–542, 2008. doi:10.1038/nrm2434.
44. **Papinski D, Kraft C.** Regulation of autophagy by signaling through the Atg1/ULK1 complex. *J Mol Biol* 428: 1725–1741, 2016. doi:10.1016/j.jmb.2016.03.030.
45. **Penafuerte CA, Gagnon B, Sirois J, Murphy J, MacDonald N, Tremblay ML.** Identification of neutrophil-derived proteases and angiotensin II as biomarkers of cancer cachexia. *Br J Cancer* 114: 680–687, 2016. doi:10.1038/bjc.2016.3.
46. **Pickrell AM, Youle RJ.** The roles of PINK1, parkin, and mitochondrial fidelity in Parkinson's disease. *Neuron* 85: 257–273, 2015. doi:10.1016/j.neuron.2014.12.007.
47. **Raben N, Hill V, Shea L, Takikita S, Baum R, Mizushima N, Ralston E, Plotz P.** Suppression of autophagy in skeletal muscle uncovers the accumulation of ubiquitinated proteins and their potential role in muscle damage in Pompe disease. *Hum Mol Genet* 17: 3897–3908, 2008. doi:10.1093/hmg/ddn292.
48. **Raben N, Wong A, Ralston E, Myerowitz R.** Autophagy and mitochondria in Pompe disease: nothing is so new as what has long been forgotten. *Am J Med Genet C Semin Med Genet* 160C: 13–21, 2012. doi:10.1002/ajmg.c.31317.
49. **Roach PJ.** AMPK → ULK1 → autophagy. *Mol Cell Biol* 31: 3082–3084, 2011. doi:10.1128/MCB.05565-11.
50. **Romanello V, Sandri M.** Mitochondrial quality control and muscle mass maintenance. *Front Physiol* 6: 422, 2016. doi:10.3389/fphys.2015.00422.
51. **Russell RC, Tian Y, Yuan H, Park HW, Chang YY, Kim J, Kim H, Neufeld TP, Dillin A, Guan KL.** ULK1 induces autophagy by phosphorylating Beclin-1 and activating VPS34 lipid kinase. *Nat Cell Biol* 15: 741–750, 2013. doi:10.1038/ncb2757.
52. **Russell RC, Yuan HX, Guan KL.** Autophagy regulation by nutrient signaling. *Cell Res* 24: 42–57, 2014. doi:10.1038/cr.2013.166.
53. **Sanders PM, Russell ST, Tisdale MJ.** Angiotensin II directly induces muscle protein catabolism through the ubiquitin-proteasome proteolytic pathway and may play a role in cancer cachexia. *Br J Cancer* 93: 425–434, 2005. doi:10.1038/sj.bjc.6602725.
54. **Sandri M.** Protein breakdown in cancer cachexia. *Semin Cell Dev Biol* 54: 11–19, 2016. doi:10.1016/j.semcdb.2015.11.002.
55. **Sandri M.** Protein breakdown in muscle wasting: role of autophagy-lysosome and ubiquitin-proteasome. *Int J Biochem Cell Biol* 45: 2121–2129, 2013. doi:10.1016/j.biocel.2013.04.023.
56. **Scarpulla RC, Vega RB, Kelly DP.** Transcriptional integration of mitochondrial biogenesis. *Trends Endocrinol Metab* 23: 459–466, 2012. doi:10.1016/j.tem.2012.06.006.
57. **Sebastián D, Sorianello E, Segalés J, Irazoki A, Ruiz-Bonilla V, Sala D, Planet E, Berenguer-Llergo A, Muñoz JP, Sánchez-Feutrie M, Plana N, Hernández-Álvarez MI, Serrano AL, Palacín M, Zorzano A.** Mfn2 deficiency links age-related sarcopenia and impaired autophagy to activation of an adaptive mitophagy pathway. *EMBO J* 35: 1677–1693, 2016. doi:10.15252/embj.201593084.
58. **Semprun-Prieto LC, Sukhanov S, Yoshida T, Rezk BM, Gonzalez-Villalobos RA, Vaughn C, Michael Tabony A, Delafontaine P.** Angiotensin II induced catabolic effect and muscle atrophy are redox dependent. *Biochem Biophys Res Commun* 409: 217–221, 2011. doi:10.1016/j.bbrc.2011.04.122.
59. **Song YH, Li Y, Du J, Mitch WE, Rosenthal N, Delafontaine P.** Muscle-specific expression of IGF-1 blocks angiotensin II-induced skeletal muscle wasting. *J Clin Invest* 115: 451–458, 2005. doi:10.1172/JCI22324.
60. **Springer W, Kahle PJ.** Regulation of PINK1-Parkin-mediated mitophagy. *Autophagy* 7: 266–278, 2011. doi:10.4161/auto.7.3.14348.
61. **Tabony AM, Yoshida T, Galvez S, Higashi Y, Sukhanov S, Chandrasekar B, Mitch WE, Delafontaine P.** Angiotensin II upregulates protein phosphatase 2Cα and inhibits AMP-activated protein kinase signaling and energy balance leading to skeletal muscle wasting. *Hypertension* 58: 643–649, 2011. doi:10.1161/HYPERTENSIONAHA.111.174839.
62. **Triolo M, Hood DA.** Mitochondrial breakdown in skeletal muscle and the emerging role of the lysosomes. *Arch Biochem Biophys* 661: 66–73, 2019. doi:10.1016/j.abb.2018.11.004.
63. **Ylä-Anttila P, Vihinen H, Jokitalo E, Eskelinen EL.** Monitoring autophagy by electron microscopy in mammalian cells. *Methods Enzymol* 452: 143–164, 2009. doi:10.1016/S0076-6879(08)03610-0.
64. **Yoshida T, Delafontaine P.** Mechanisms of cachexia in chronic disease states. *Am J Med Sci* 350: 250–256, 2015. doi:10.1097/MAJ.0000000000000511.
65. **Yoshida T, Semprun-Prieto L, Sukhanov S, Delafontaine P.** IGF-1 prevents ANG II-induced skeletal muscle atrophy via Akt- and Foxo-dependent inhibition of the ubiquitin ligase atrogin-1 expression. *Am J Physiol Heart Circ Physiol* 298: H1565–H1570, 2010. doi:10.1152/ajpheart.00146.2010.
66. **Yoshida T, Semprun-Prieto L, Wainford RD, Sukhanov S, Kapusta DR, Delafontaine P.** Angiotensin II reduces food intake by altering orexigenic neuropeptide expression in the mouse hypothalamus. *Endocrinology* 153: 1411–1420, 2012. doi:10.1210/en.2011-1764.
67. **Zhang L, Du J, Hu Z, Han G, Delafontaine P, Garcia G, Mitch WE.** IL-6 and serum amyloid A synergy mediates angiotensin II-induced muscle wasting. *J Am Soc Nephrol* 20: 604–612, 2009. doi:10.1681/ASN.2008060628.